Hindawi
Geofluids
Volume 2022, Article ID 9424120, 22 pages
https://doi.org/10.1155/2022/9424120

Research Article

Study on Crack Evolution and Failure Mechanism of Fully Penetrated Fracture Grouting Body

Hanqing Wang,[1] Li Li,[2] Xinwang Li,[1,3] Lichao Cheng,[1,3] and Pengfei Shen [1,4,5]

[1]*School of Mining Geomatics Engineering, Hebei University of Engineering, Handan 056038, China*
[2]*School of Civil Engineering, Hebei University of Engineering, Handan 056038, China*
[3]*Coal Resources Development and Construction Application Technology Research Center of Universities in Hebei Province, Hebei University of Engineering, Handan 056038, China*
[4]*Guangdong Provincial Key Laboratory of New and Renewable Energy Research and Development, Guangzhou 510640, China*
[5]*State Key Laboratory of Oil and Gas Reservoir Geology and Exploitation (Southwest Petroleum University), Chengdu 610500, China*

Correspondence should be addressed to Pengfei Shen; shenpengfei@hebeu.edu.cn

Received 18 August 2022; Accepted 22 September 2022; Published 10 October 2022

Academic Editor: Yu Wang

Grouting is a common method used in reinforcing fractured rock, and it is important to study the crack evolution and mechanical properties of fractured rock after grouting under the influence of different excavation rates and crack geometries. Therefore, a set of grouting molds for small-sized specimens with fully penetrated cracks were designed. The crack formation location and penetration mechanism of grouted bodies with different crack inclinations using uniaxial compression tests with different loading rates were investigated. The crack extension process and energy concentration areas of the grouted plus solid specimens at different stages were revealed from the acoustic characteristic. The results show that the peak strength of crack-grouting sandstone decreases with the increase of crack inclination under the same loading rate. Comparisons of the crack inclination in slurry specimens under different loading rates imply that there is a critical value of crack inclination at 45° which concentrates the damage and cracking of the grouted body under compression within the grouted solidified body. When the crack inclination is small, the specimen is mainly extended from the crack of the rock block at the upper end of the grout consolidation to the lower end of the crack surface, and the acoustic emission ring count data mainly show a rising trend throughout the whole process, when the crack inclination is large, cracks are mainly produced around the surface subjected to grout consolidation and gradually expand to the interior of the grouted body, and there is almost zero growth in the ringing count in the elastic stage (II) and a larger growth in the ringing count in the yielding stage (III) and postpeak stage (IV). This research work can provide disaster prediction and theoretical guidance for the corresponding engineering construction of crack-grouting sandstone.

1. Introduction

Fissures are prevalent and randomly distributed in most rock masses in nature, and these fissures exist across different spatial scales and forms in the rock mass. They reduce the strength of the rock mass and play a dominant role in controlling the deformation, damage, and stability of the rockwork [1, 2]. To prevent the continued extension of fissures and construction safety, the stress state of the rock is fundamentally changed by injecting slurry into the pores and fissures. Cement grouting is a common means of reinforcement in rock engineering operations, such as slope support, dam foundation treatment, tunnel excavation, and overburden off-layer grouting in mining [3–6]. Compared with other rock reinforcement techniques [7, 8], cement grouting has the advantages of reliable application, simplicity of application, and ecofriendliness and does not require complex construction equipment. Therefore, the study of

cement grouting has high scientific significance and application value in rock engineering [9–12].

Different crack forms after grouting reinforcement form a new "complete whole" with complex mechanical properties and stress distribution characteristics. In recent decades, many scholars have been devoted to the investigation of specimens after grouting reinforcement of different jointed fractured rock masses, and strength and crack expansion patterns under different stress states were studied by several methods. Lu et al. investigated the effects of grouting thickness on the mechanical properties of structural rock containing prefabricated serrated crack surfaces by direct shear tests [13]. Zhou et al. selected four rock materials as samples to study the damage behavior of reinforced rock mass under dynamic cyclic loading. It is found that the damage variables of rock mass at different peak strength ratios vary with strain rates [14]. Le et al. performed comparisons of compressive strength, damage mode, and deformation properties of grout-filled crack specimens and unfilled fracture specimens under different geometries using uniaxial compression tests. Grout injection reinforcement was found to be able to greatly improve the shear strength of the rock and slurry bond [15, 16]. Xu et al. evaluated the effects of grouting on the crack expansion pattern and strength of specimens. The crack pattern and stiffness magnitude of the specimen were found to be related to the strength of the grouting material, and the strength of the specimen increases with the strength of the grouting material [17]. Sharafisafa et al. studied prefabricated crack-like rock specimens after filling, and the results showed that the filled specimens could withstand greater loads before damage [18]. The effects of different inclination angles and loading rates on coal fracture mechanics are studied by Wu et al. by using compression and shear tests. It is found that the peak strength decreases with the increase of loading rate when the inclination angle of fracture is small [19]. Bao et al. explored the influence of loading rate on the Hoek-Brown failure criterion of andesite. The results showed that the compressive strength and tensile strength of the form axis were not related to the loading rate and water saturation, and the correlation between water saturation and loading rate of the failure criterion could be mutually converted [20]. Weng et al. performed grout penetration tests of fractured sandstone specimens by use of the NMR technique, and the slurry injection volume and filling rate were studied in terms of surrounding pressure, different temperatures, and number of cracks [21]. From the degree of fractured rock damage after grouting, these methods can reveal the damage mechanism of crack morphology at different scales under the same stress regime [22, 23]. However, in practice, the excavation rate will induce a series of engineering disasters such as rock bursts and collapses. Therefore, more consideration should be given to the macromechanical properties and damage patterns resulting from the combination of complex crack distribution types and excavation rates in the rock mass. For example, the mechanical properties and damage crack response of various crack-bearing rock masses were examined under various loading rates and multistage cyclic loading conditions, it is believed that an increase in loading rate leads to an increase in crack length, and the rock damage intrinsic model of loading rate effect is established [24]. In some recent studies, Kumar et al. fabricated four types of postgrouting specimens and investigated crack behavior of the specimens at different strain rates and two crack inclinations, it is concluded that the strain rate has a significant effect on the mechanics of intact and crack-containing specimens, and specimens loaded rapidly are mainly subject to tensile and shear damage [25]. The morphology of prefabricated cracks determines the generation and expansion of cracks. The mechanical properties and cracking behavior of rock and land are studied by Wang et al. by using cyclic triaxial loading test; it is found that the volume deformation of rock gradually decreases with the increase of block content, confining pressure strength, and stiffness. However, the stress state of the soil changed under the influence of confining pressure, and the surrounding multiple interface cracking behaviors occurred [26, 27]. Acoustic emission characteristics are considered to be an effective means to monitor the process of rock breaking, so herein, acoustic emission technology is also widely used to provide disaster prediction for the construction of the corresponding fissure grouting rockwork. Cao et al. carried out uniaxial compression test and acoustic emission monitoring test of rock specimens under different mining loading rates from the point of view of impact hazards associated with coal rock mining, and the increase in loading rate was found to reduce the number of acoustic emission event points [28]. Ai et al. undertook localization experiments using acoustic emission event counts and revealed the spatiotemporal evolution of coal deformation and damage under different loading rates, and a quantitative analysis of the precursor characteristics of coal body damage was performed [29]. Jiang et al. estimated the effects of edge crack length and location on the acoustic emission characteristics of rock specimens containing edge cracks, and the crack location was found to affect the acoustic emission data to a lesser extent than the crack length [30]. The triaxial compression acoustic emission monitoring tests on crack-bearing rock specimens was conducted at different loading rates. The effects of surrounding pressure and loading rate on the acoustic emission activity and damage characteristics of the specimens were determined [31–33].

According to the findings in the above study, although a large number of experimental studies on grouting of fractured rock specimens have been conducted in the past, the focus remains on the influence of crack geometry in many studies. The crack inclination involved is relatively singular and most of cracks are not full-penetration cracks. For considering the loading rate and the damage characteristics of prefabricated cracks on the rock mass, researchers focused on the study of fractured rock without filling and grouting. The mechanical properties and damage patterns of rock specimens after filling and grouting under the influence of the combination of loading rate and crack inclination are less frequently reported. Therefore, uniaxial compression tests and acoustic emission monitoring equipment were used to further reveal the damage mechanism of fractured grouted sandstone at different loading rates and different fracture inclination angles.

2. Experiments

2.1. Specimen Preparation. This test specimen was selected from the sandstone in Zigong area of Sichuan; the specimen is light red, with good homogeneity. The main physicomechanical parameters are listed in Table 1. Rock specimen sizes are in accordance with ASTM D7012-2010 [34], and specimens were formed into cylinders by rock coring machine and a CNC stone grinding machine to measure Φ 100mm × 50 mm, and the flatness of the contact surface of the specimen under pressure is less than 0.02 mm. Prefabricated cylindrical specimens with five different fissure inclinations were used in the study using a laboratory CNC cutting machine (of 0°, 15°, 30°, 45°, and 60°, respectively). A prefabricated fully penetrated crack grouted specimen and acoustic emission probe arrangement location schematic diagram can be seen in Figure 1. The shaded part of the figure indicates the cement-filled block, the width of the fissure is uniformly 5 mm, and the fracture plane is a regular plane. In accordance with the "Grouting Construction Manual" [35], the grouting material is prepared at a water-cement ratio of 0.5, and the cement used in the test is 42.5 ordinary silicate cement.

2.2. Design and Application of Fractured Rock Specimen Grouting Mold. Acrylic sheet was used as raw material, and the laser cutting machine is used to produce the inner diameter of 48 mm and outer diameter of 50 mm, in a semicircular mold with a height of 100 mm. The design of this size can better ensure the specimen crack integrity, and the surface of the specimen is closed with Plexiglas to prevent slurry from leaking out. The grouting port at the fissure corresponding to the grouting mold was drilled, and the rubber tube in the grouting port was set, and glue was set to fix the connection between the grouting port and the rubber tube. When injecting slurry, a syringe can be used to connect the other end of the rubber tube to inject cement slurry all over the fissure surface. The whole grouting process and the effect are shown in Figure 2.

The above method was used to obtain sandstone fissure grouted solid specimens with different fissure inclination angles. The specimens were grouted 24 h after demolding in an indoor environment and wrapped with cling film, with water applied for 28 d after the uniaxial compression test to facilitate curing. The process is shown in Figure 3; a red sandstone crack grouted body (at 28 d) is illustrated in Figure 4.

2.3. Test Equipment and Loading Conditions. The test equipment consists of a loading system, image monitoring system, and acoustic emission acquisition system (Figure 5). Loading equipment using a KYAG-600 type microcomputer-controlled rock rigidity testing machine makes force control or displacement control possible. By adjusting the height of the tester base disc, it is possible to make full contact between the compressed surface of the specimen and the upper indenter, to reduce the effect of test piece flatness. The image detection system was based on a Canon EOS200D high-speed digital camera with a video shooting resolution of 1920 × 1080 pixels, at a frame rate of 25-30 frames per second.

Table 1: Basic mechanical parameters of sandstone.

Density ($kg\,m^{-3}$)	Compressive strength (MPa)	Modulus of elasticity (GPa)	Modulus of deformation (GPa)
2389	14.3~21.8	1.4~2.1	0.817~1.068

The acoustic emission equipment is selected from the PCI-2 multichannel acoustic emission system (American Acoustic Co., USA). Four acoustic emission probes were arranged around the specimen before the test, acoustic emission probes crossed in the middle and lower part of the specimen as determined by the lead break test (Figure 1), and petroleum jelly was applied to the contact area between the probe and the specimen to achieve coupling between the two. After repeated debugging and external noise shielding, the threshold value was set to 40 dB. Uniaxial compression tests used displacement control at a loading rate of 0.005 mm/s, 0.01 mm/s, 0.03 mm/s, and 0.05 mm/s, respectively. To reduce the effect of specimen discretization on the results, three tests were conducted at each loading rate, and the data on the test machine and the acoustic emission signal data were recorded at the same time.

3. Experimental Results

3.1. Analysis of Mechanical Characteristics of Grouting under Different Loading Rates. Figure 6(a) shows the variation law of peak strength of fracture-grouting mass under different loading rates. It can be found that the peak strength of crack-grouting sandstone specimen increases slightly with the increase of loading rate when the crack inclination is between 0° and 45°. However, the peak strength of crack-grouting sandstone decreases with the increase of loading rate when the crack inclination is 60°. Especially when the loading rate is 0.05 mm/s and the crack inclination angle is 60°, the peak strength is the lowest, which is only 14.6% of that of the complete specimen. In addition, at the same loading rate, the peak strength of sandstone-fractured grout sample decreases with the increase of fracture dip angle. Except that the peak strength of the specimen with the crack inclination angle of 60°decreases greatly, the peak strength of other specimens increases with the increase of loading rate when the crack inclination angle is the same.

Figure 6(b) shows the variation law of deformation modulus of fractured grout under different loading rates. It can be seen that the deformation modulus of the fractured grouting body changes obviously compared with the intact original rock, and the overall trend is decreasing. Among them, when the fracture inclination is 60°and the loading rates are 0.03 mm/s and 0.05 mm/s, the minimum deformation modulus is 0.330 GPa, which is only 30% of the complete specimen. Under the same loading rate, the deformation modulus decreases with the increase of crack inclination. This is mainly because the crack surface first bears axial stress in the compression process of the specimen. The lateral shear strength along the fracture surface decreases with the crack inclination increases, making its slip deformation

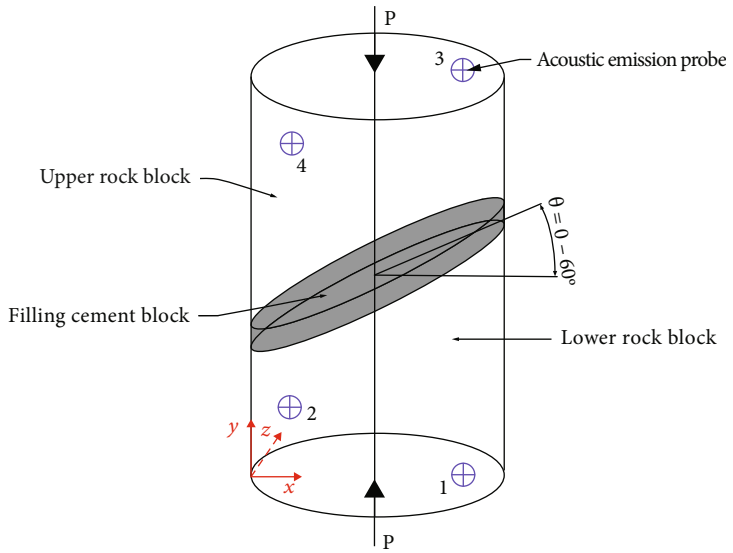

Figure 1: Schematic diagram of the fully penetrated crack grouted body.

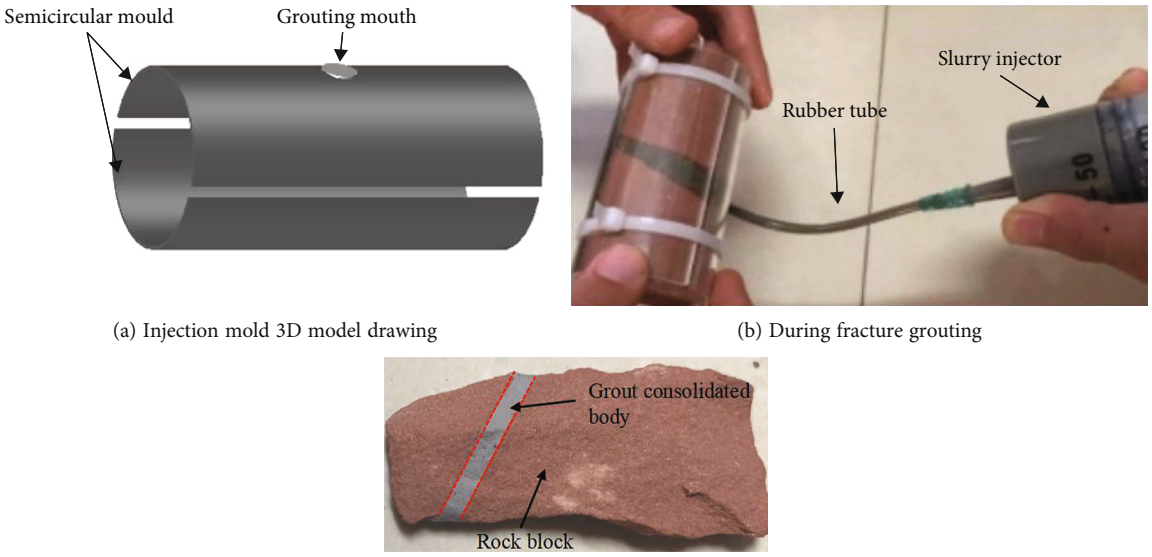

(a) Injection mold 3D model drawing

(b) During fracture grouting

(c) Internal effect after fracture grouting

Figure 2: Indoor grouting process and effect of standard fractured rock.

larger. When the crack inclination angle is 0°~45°, the deformation modulus of sandstone-fractured grout decreases with the increase of fracture inclination angle. When the crack inclination angle is 60°, the deformation modulus decreases with the increase of loading rate, which is consistent with the change characteristics of peak strength. This is because when the crack inclination angle is large, the slip failure of the crack grouting surface is relatively sufficient and the deformation failure is large. In addition, with the increase of loading rate, the strain value corresponding to the specimen reaching the peak strength is shortened, mainly showing brittle failure, and the transverse and axial deformation is small, resulting in the gradual increase of deformation modulus with the increase of loading rate.

Through the above results, it is found that the existence of cracks will make the peak strength of grouted specimens deteriorate in different degrees. In this paper, the deterioration coefficient is introduced to quantitatively study the deterioration characteristics of the peak strength of grouted specimens caused by the dip angle of cracks. The expression of its deterioration coefficient ω is as follows [36]:

$$\omega = 1 - \frac{\sigma_s}{\sigma_o}, \tag{1}$$

where σ_s is the peak strength of grout specimen with cracks at the same loading rate and σ_o is the peak strength of complete specimen. From the formula, it can be seen that the greater the deterioration coefficient, the smaller the peak strength of the grout specimen, and conversely, the smaller the attenuation degree, the closer it is to the strength of the complete specimen.

Figure 3: Indoor environment, cling film wrapped specimen watering maintenance.

Figure 4: Red sandstone crack grouted body specimens.

Figure 7 shows the relationship curve between the deterioration coefficient of crack-grouting sandstone and the crack inclination. It can be seen that the deterioration coefficient increases with the increase of crack inclination under the same loading rates. When the deterioration coefficient of the specimen reaches the maximum value and the minimum value, the crack inclination is 60° and 0°, respectively. This shows that the deterioration coefficient of the specimen shows a positive correlation with the crack inclination. However, the influence of different loading rates on the deterioration coefficient of specimens does not show regularity under the same crack inclination.

3.2. Analysis of Macroscopic Crack Morphology of Grouted Body. Figure 8 shows the final damage morphology of the grouted body with different crack inclinations at a loading rate of 0.01 mm/s, with the increase of crack inclination, the development form of cracks in the grouted body specimen during the compression process gradually concentrates towards the crack surface, and the greater the overall damage degree of the grouted surface. In Figure 8(a), the specimen with a crack inclination angle of 0° is more similar to the uniaxial compression test damage pattern of the intact specimen (Figure 8(f)), which shows an overall V-shaped shear damage pattern, mainly arising from the common development of two lateral inclined shear cracks extending to the lower end of the grouting surface and accompanied by local rock block detachment. Figure 8(b) displays that the final damage of the specimen with a crack inclination angle of 15° is first formed by a reverse wing crack on the pressurized surface and penetrates the crack surface, as the applied load is increased, because the strength of the grouting material is greater than the strength of the sandstone, the sandstone breaks before the grouting consolidation surface, and the edges of the crack surface and the lower end of the shedding, bulging, and axial cracking occur, which develops rapidly, causing a loss of bearing capacity. From Figure 8(c), it can be seen that the overall performance of the specimen with a crack inclination angle of 30° is mainly axial crack damage, subject to axial loading at the upper end of the crack surface first formed perpendicular to the pressure surface cracks, and as the load increases, the internal cracks of the grouted body continue to develop, and then, the compressive stress propagates to the lower end of the specimen, thus forming more obvious axial cracks. From Figures 8(d) and 8(e), compared to the specimens with crack inclination angles of 0°, 15°, and 30°, the cracks in the 45° specimen exist mainly inside the grouting surface and form very few axial cracks running from the crack surface, the 60° specimen was damaged by direct slip shear from the crack surface, and there is a small amount of dislodgement of the grouted solids, but no visible cracks in other parts.

According to the above analysis results, the final damage morphology of the specimens under different loading rate conditions was specifically analyzed by taking the crack inclination angles 30° and 45° grouted body specimens as an example (Figure 9). With the increasing loading rate, the damage form of the grouted specimen changes from local damage destabilization to full damage destabilization; the latter is mainly manifested in the greater degree of damage at the grouting surface, which is more likely to cause instantaneous destabilization of the specimen, as evinced by the number of cracks and the degree of penetration, while its damage form changes from axial splitting to shear damage. The specific analysis is described as follows:

(1) For the specimen with the crack inclination angle of 30°, the displacement rate is 0.005 mm/s, and the new cracks of the grouted body occur mainly at the upper end of the crack surface, extend to the crack surface, and stop at the crack surface which does not develop. The reason for this is that the strength of the grouting material (42.5 ordinary silicate cement) is higher than that of the sandstone, and the upper rock reaches the compressive strength first before the grouted body is completely destroyed under this low loading rate; when the displacement rate is 0.01-0.05 mm/s, the crack development on the grouting surface increases as the loading rate increases, the cracks develop toward the lower end of the crack surface, axial splitting damage is dominant, and a certain degree of crack-opening develops

(2) For the specimen with the crack inclination angle of 45°, at displacement rates of 0.005 mm/s and 0.01 mm/s, the cracks are generated inside the

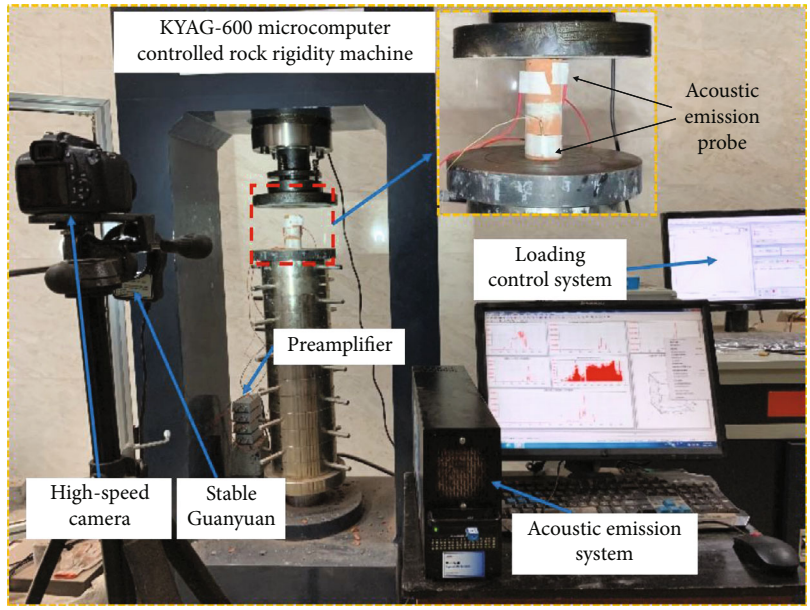

Figure 5: Sandstone test data acquisition system diagram.

specimen and inside the grouted body, and the damage pattern is mainly manifested in the formation of multiple axial cracks around the crack surface, accompanied by a small number of parallel to the direction of crack inclination. When the displacement rate is 0.03 mm/s, the cracks are mainly produced in and around the grouted body, a few small cracks appear on the surface of the specimen, the expansion direction is parallel to the inclination direction, and part of the grouted body is dislodged; at a displacement rate of 0.05 mm/s, the damage pattern is mainly characterized by severe shear slip damage along the crack surface, with the main crack located inside the grouted body and parallel to the inclination angle. The reason for this is that an increase in loading rate leads to a decrease in the shear strength at the interface between the crack surface and the grouted body

In summary, at a given load rate, the crack tilt angle is 0°, 15°, and 30°, the crack development of the grouted specimen is more adequate, and its damage pattern is more akin to that of the intact specimen; when the crack inclination angle is 45° or 60°, it basically maintains the direct damage by the grouting surface and does not cause obvious cracks to the specimen as a whole; for a crack inclination of 30°, the number of cracks formed increases as the loading rate increases, while the opposite is true for the crack inclination 45° specimen. It can be seen that there is a critical value of 45° of crack inclination that concentrates the cracks inside the grouted body and produce shear damage, causing a loss of bearing capacity; for small crack inclination angles, grouting consolidation at low loading rate can play a role in inhibiting crack expansion, whereas when the crack inclination angle is larger, the cracks expand along the crack surface towards the upper and lower ends of the specimen at low loading rate, and the cracks are mainly concentrated inside the grouted body at high loading rates.

3.3. The Evolution of Cracking of the Injected Body. According to the conclusion in Section 3.2, there is a critical value of 45° of crack inclination that makes a difference in the damage crack expansion pattern of the grouted body during the compression process. In this section, specimens with crack inclination angles of 30° and 45° will be used as examples to analyze more specifically the fine damage characteristics and the intrinsic mechanism of the fissure-containing rock mass after grouting reinforcement at the same loading rate.

Figure 10 shows typical screenshots and stress-time relationships during the cracking of the grouted specimens at a loading rate of 0.03 mm/s and a crack inclination of 30°. Figure 10(b) indicates that two nascent cracks are formed at point A before the peak, and the axial compressive stress increases with time; at point C and point B, five cracks appeared at the lower and upper ends of the crack surface of the specimen, in the shape of Chinese capital letter "八" (meaning eight) towards the crack surface, as shown in Figure 10(c), until the compressive stress reaches the peak front end D point; cracks No. 1 and No. 2 penetrate and are accompanied by tiny tension cracks and shear cracks on the grouting surface, while cracks begin to appear at the lower end of the crack surface (cracks No. 13 and No. 14 in Figure 8). Cracks 2-4, 6-8-9, and 5-12 penetrate when the specimen reaches peak strength; as the compressive stress appears to fall slowly, a smaller stress drop occurs, and eventually, the surface damage of the specimen is more complete at point E, after which it enters the stage of slow crack expansion. During this period, it can be seen from the final specimen damage as sketched in Figure 10(g) that no macroscopic cracks appear in the grouted consolidation and only a small amount of localized detachment occurs.

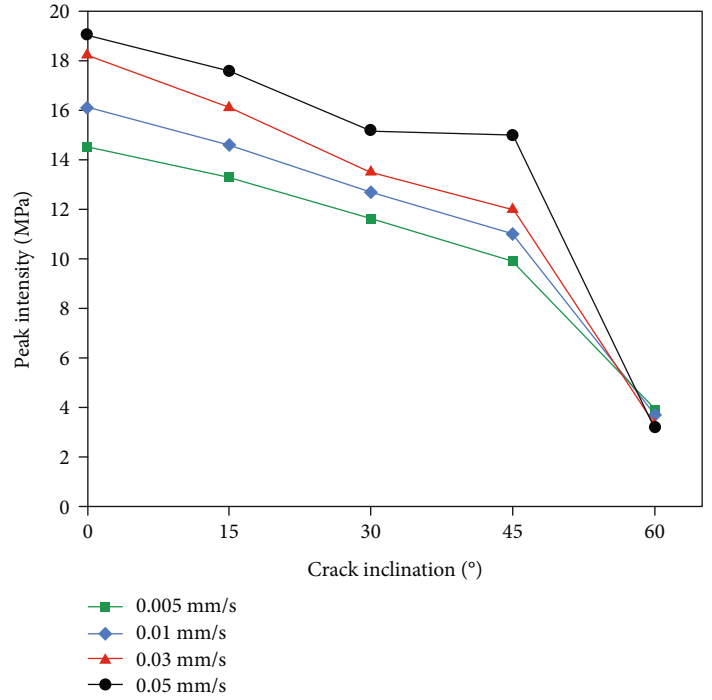

(a) Variation law of peak strength of sandstone grouting body

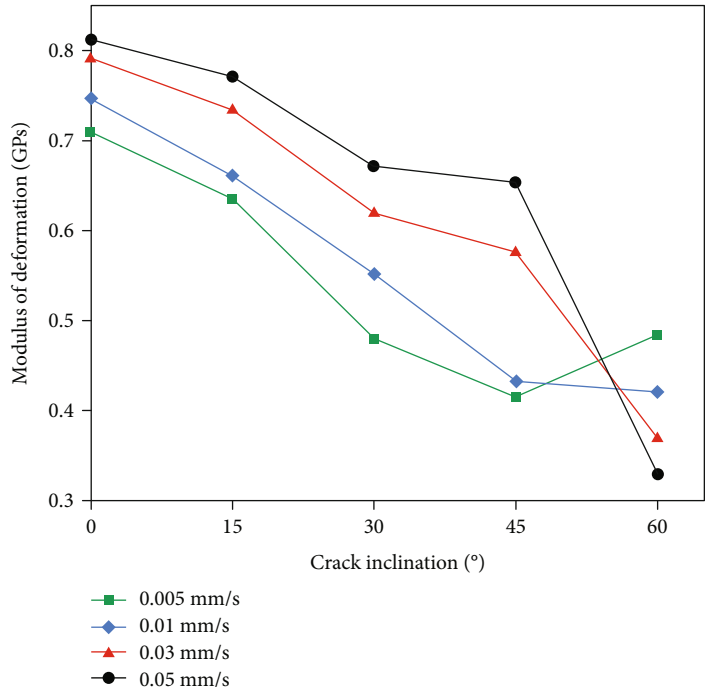

(b) Variation law of deformation modulus of sandstone grouting body

Figure 6: Variation curves of mechanical properties of grouting materials under different loading rates.

Figure 11 demonstrates typical screenshots and stress-time relationships during the fine view cracking of the grouted specimens at a displacement rate of 0.03 mm/s and a crack inclination angle of 45°. At point A before the peak, new microcracks are generated near the grouting surface, and when point A reaches point B within the time period, three new cracks appear within the grouting surface and at the upper end, respectively, and the crack direction mainly forms shear damage along the crack surface. With increasing stress, three axial cracks (Nos. 7-9) are derived at point C. Meanwhile, cracks 1-6 begin to develop and expand along the crack inclination in the form of similar goose-like cracks, at which time the grouting surface begins to break down, resulting in stress mainly being concentrated on the crack

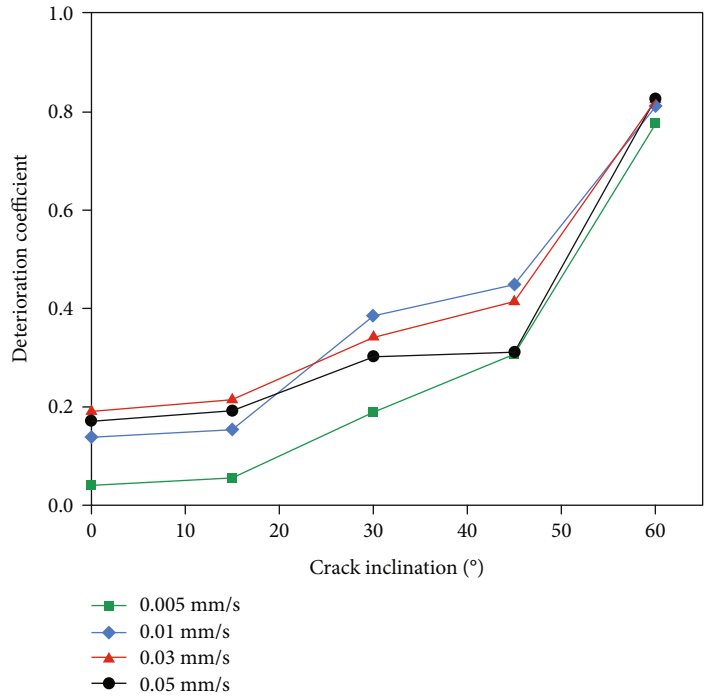

Figure 7: Relation curve between deterioration coefficient of crack-grouting sandstone and crack inclination.

surface; when the peak is reached, tiny cracks inside the crack surface begin to arise at point D (cracks 10-12); subsequently, the stress appears to decline slowly until point E, but this is still accompanied by the generation of cracks (13 and 14), and these are mainly concentrated on the grouting surface, after which it enters the frictional slip phase, due to the effect of shear damage, local bulging, and local dislodgment of the rock blocks near the inclination angle along the fissure occurs. It is noteworthy that the axial cracks (7 and 9) do not continue to expand towards the lower end of the crack face in the time after point C, which is diametrically opposed to the crack development pattern of the specimen with the crack inclination of 30°. This phenomenon is due to the fact that when the crack is produced by the action of compressive stress at the upper end of the crack surface, at this time the, stress is mainly concentrated inside the grouted body, and because the compressive strength of the grout material is higher than that of the complete sandstone specimen, smaller axial cracks form at the lower end of the crack surface in a short time. As loading continues, the prefabricated crack surface loses its load-bearing capacity, and the grouted body specimen rapidly changes from compression-shear damage to shear damage concentrated on the crack surface, which is consistent with the view in "Structural Mechanics of Rock" [37] such that the weak surface determines the mechanical properties of the rock mass.

3.4. Acoustic Analysis of Slurry Bodies with 30° and 45° Crack Inclination. Acoustic emission ringing counts can reflect the degree of rupture of the grouted specimen during the loading process [38]. Figures 12 and 13 show the stress and ringing count curves with time during uniaxial compression for specimens with crack inclination angles of 30° and 45° under different loading rates, respectively. Since sandstone is an elasto-plastic body [39], the loading process of the grouted specimen can be divided into four stages according to the stress-time curve variation characteristics: compression-density stage (I), elastic stage (II), yield stage (III), and post-peak stage (IV). As shown in Figures 12 and 13, the acoustic emission ring count increases with time and compressive stress. In the compression density stage (I), under different loading rates, the grout specimens mainly exhibit internal pore closure, relatively small acoustic emission signal intensity, and a small overall increase in ringing count. In the elastic stage (II), the specimen with the crack inclination angle of 30° shows a linear trend of increasing ring counts as the compressive stress continues to rise, which matches the trend of the stress-time curve of the grouted specimen. This indicates that the release of strain energy continues to grow during the elastic deformation of the specimen and the overall crack development is more complete, the specimen with the crack inclination angle of 45° has almost zero growth in ring count at this stage, mainly because the crack formation in the crack inclination 45° specimen is mainly concentrated on the surface and inside of the crack surface during the compression process, and the range of crack extension is small; thus, the energy released is weak, which indirectly verifies the phenomenon described in Section 3.3. In the yielding stage (III), the ring counts of specimens with 30° and 45° crack inclination both increase to different degrees, but the intensity of ring counts of specimens with 45° inclination is sparse compared to those of specimens with 30° inclination; at the same time, the crack inclination angle of 45° has a ring count value that is much greater than specimens with a crack inclination angle of 30°. The main reason is that, on the one hand, it indicates that a large

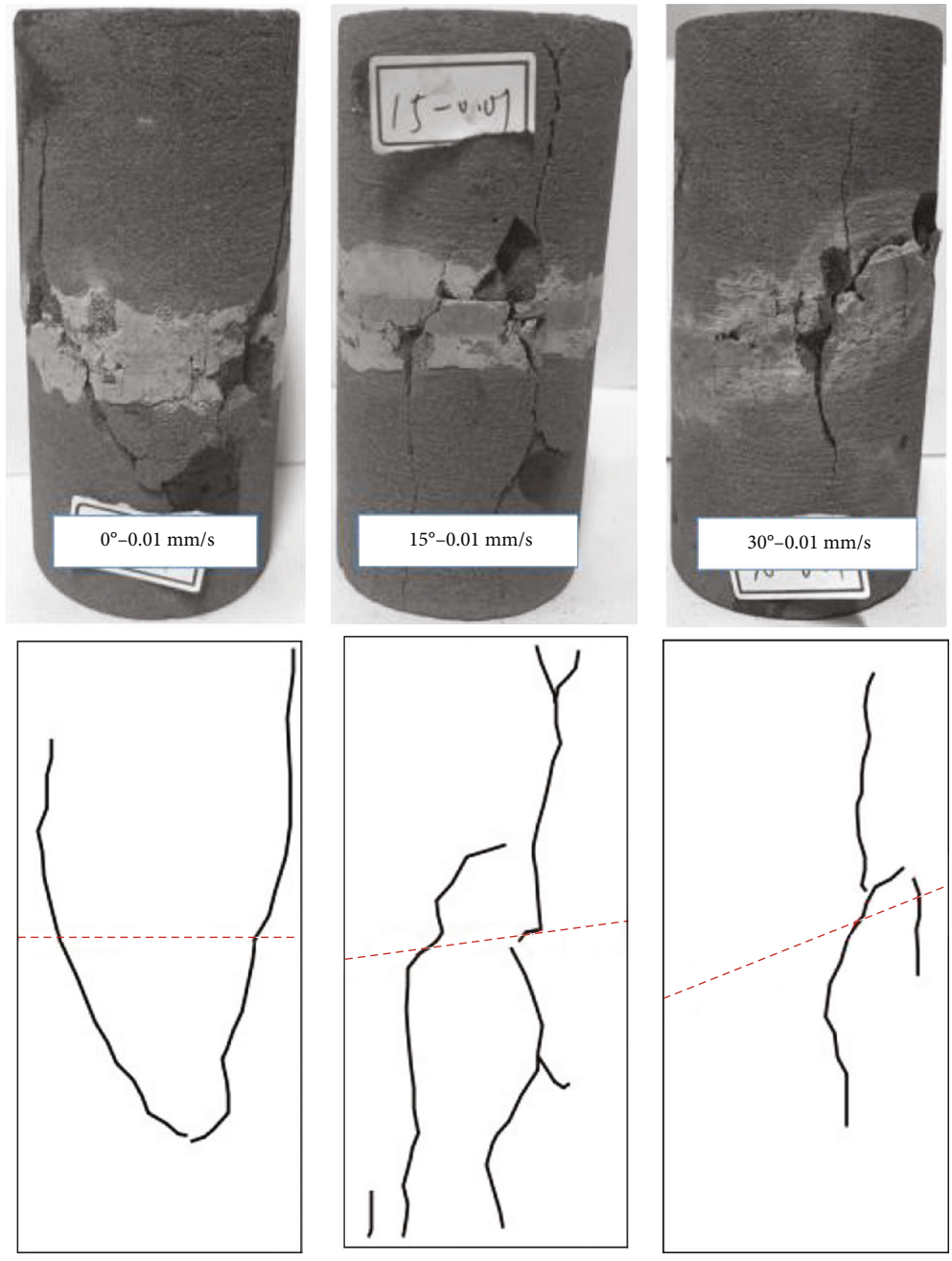

(a) 0° sample (b) 15° sample (c) 30° sample

Figure 8: Continued.

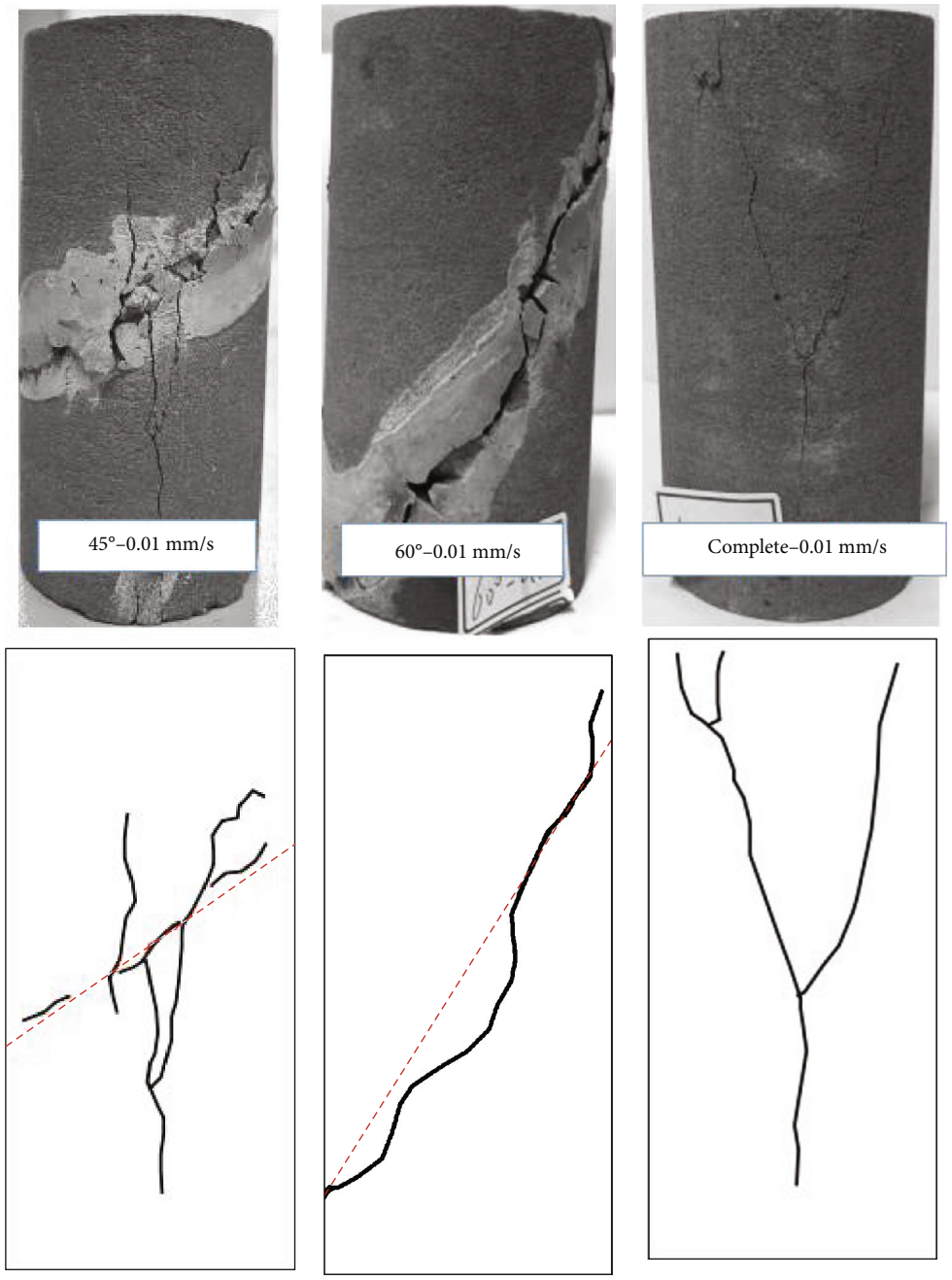

(d) 45° sample (e) 60° sample (f) Complete sample

Figure 8: Macroscopic crack damage of grouted body under different crack inclination conditions.

number of new cracks develop inside the specimen of the grouted body during the yielding stage, and with the action of compressive stress, expansion and penetration occur, and finally, the whole specimen is destroyed in the postpeak stage (IV). On the other hand, the increase of crack inclination concentrates the stress in the grouting surface, which is subject to shear damage causing a rapid loss of bearing capacity, and because the grouted body is a brittle material, when the grouted specimen reaches the peak, the grouting surface is broken and sliding damage occurs rapidly, which leads to a lower cumulative ring count.

Under uniaxial compression conditions, part of the energy change inside the grouted specimen with different loading rates and crack inclination is stored in the specimen as elastic energy, and the other part is released by the loading rate and crack inclination with the overall damage of the grouted specimen and the development of crack surface cracks [40]. Figure 14 shows the comparison of the cumulative ring counts of the specimens with crack inclination angles of 30° and 45° under different loading conditions. With the increase of the loading rate, the cumulative ring count of the specimen with the crack inclination angle of

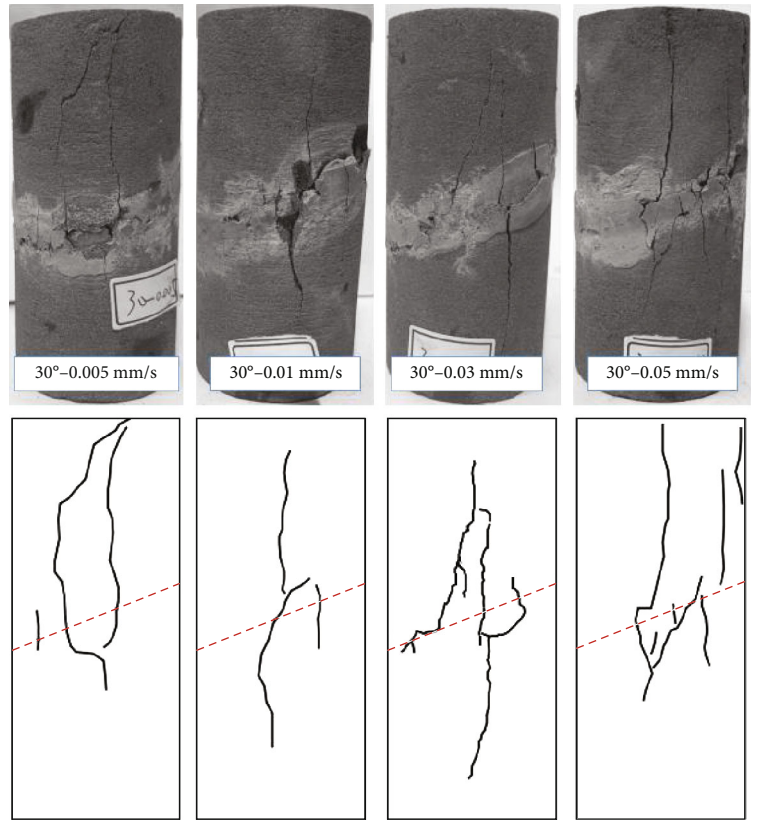

(a) The specimen with the crack inclination angle of 30°

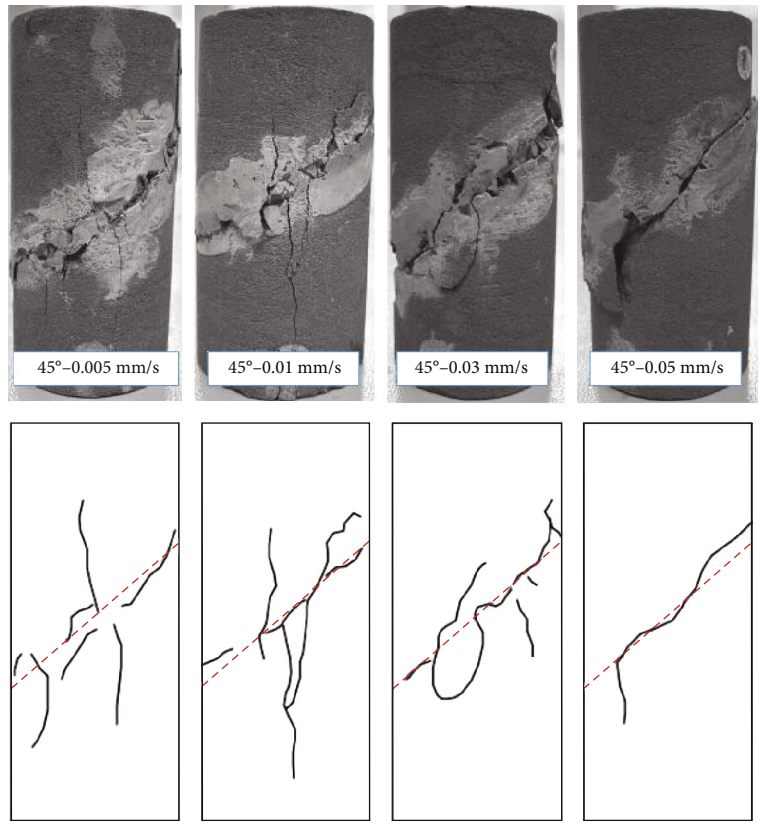

(b) The specimen with the crack inclination angle of 45°

Figure 9: Macroscopic crack damage of the grouted body under different loading rates.

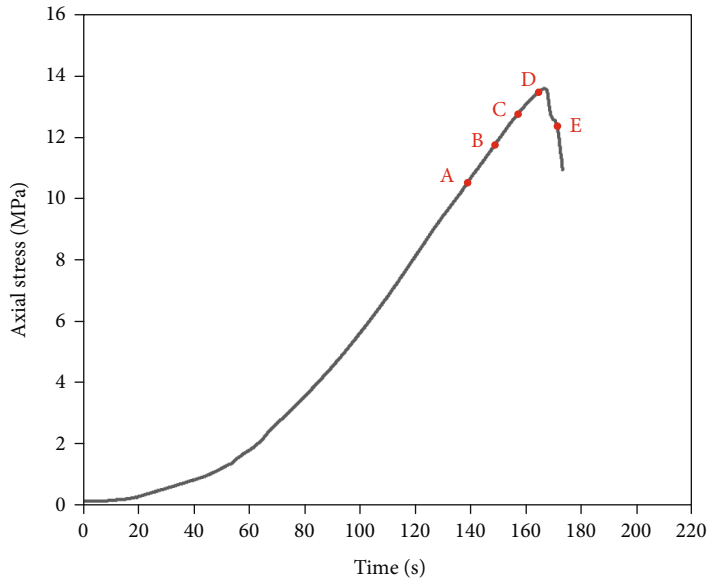

(a) Stress-time relationship for specimens with fracture inclination of 30°

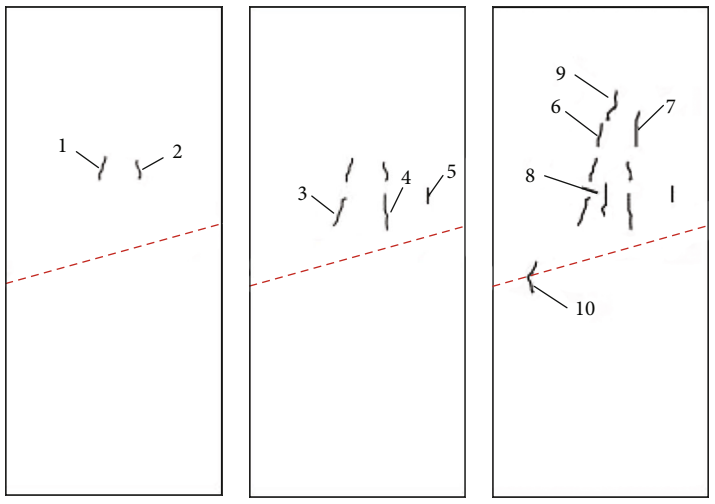

(b) Point A (136 s) (c) Point B (148 s) (d) Point C (154 s)

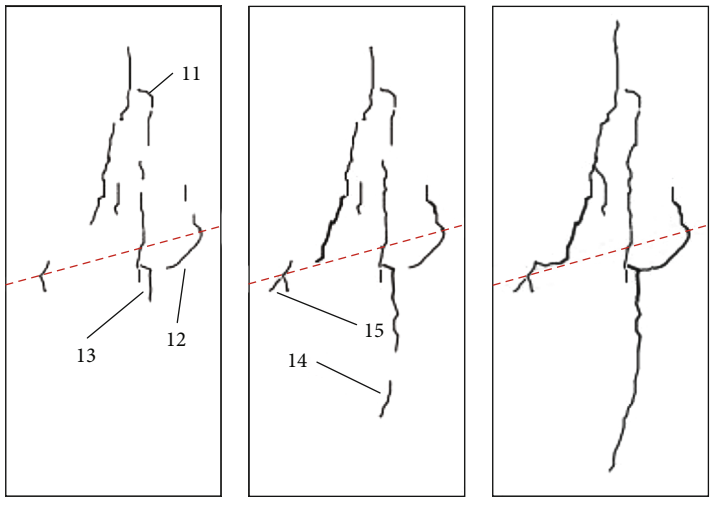

(e) Point D (164 s) (f) Point E (171 s) (g) Final damage

Figure 10: Grouted body specimen cracking extension process at a displacement rate of 0.03 mm/s and a crack inclination angle of 30°.

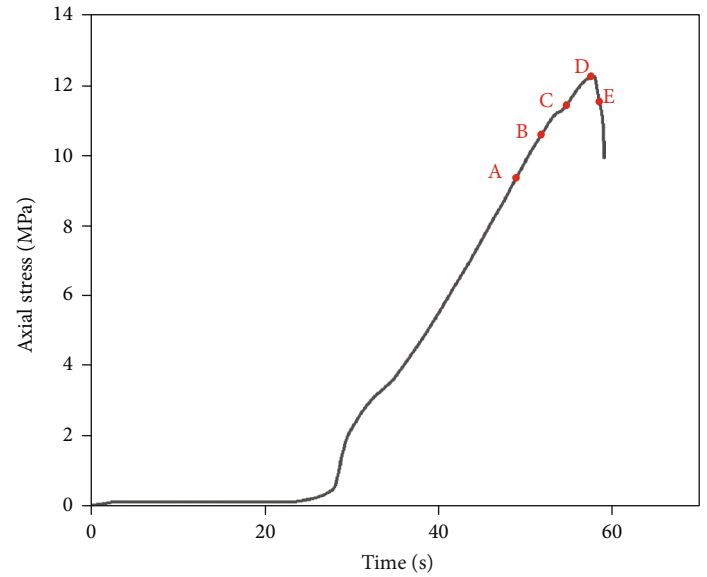

(a) Stress-time relationship for specimens with fracture inclination of 45°

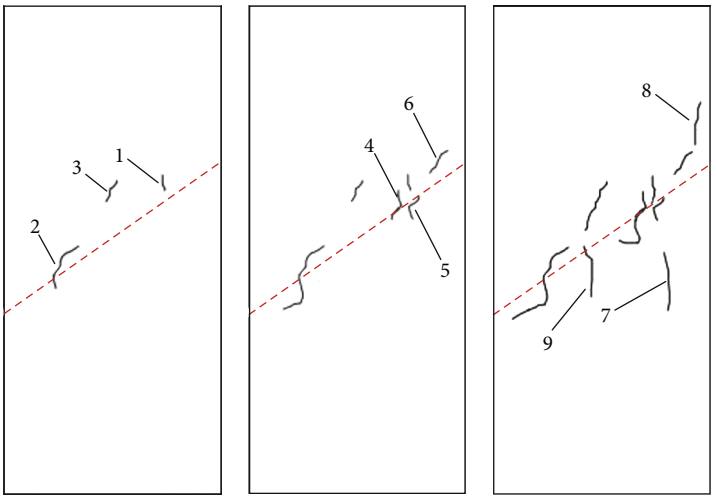

(b) Point A (46 s) (c) Point B (51 s) (d) Point C (54 s)

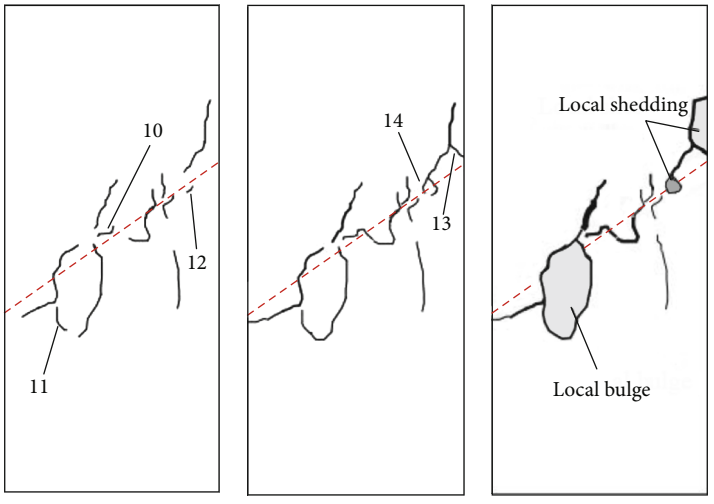

(e) Point D (58 s) (f) Point E (59 s) (g) Final damage

Figure 11: Grouted body specimen cracking extension process at a displacement rate of 0.03 mm/s and a crack inclination angle of 45°.

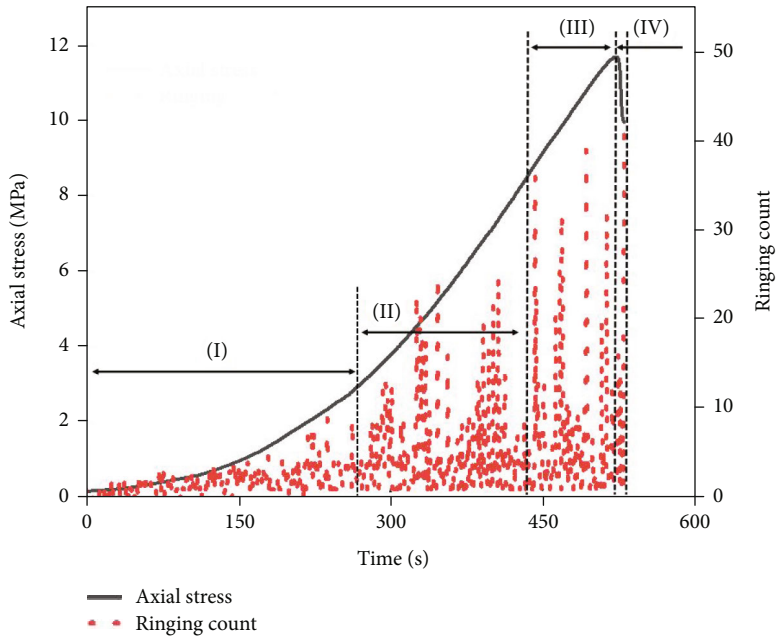

(a) Loading rate 0.005 mm/s

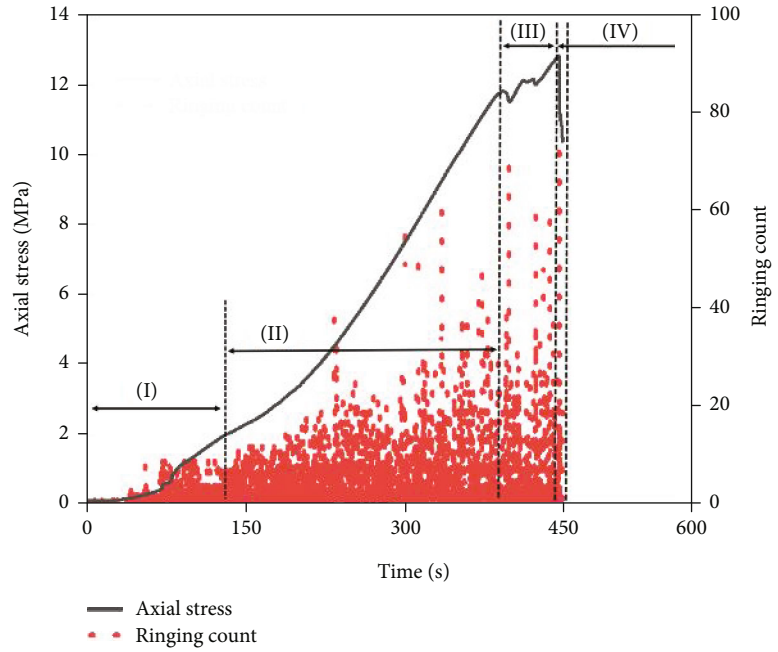

(b) Loading rate 0.01 mm/s

Figure 12: Continued.

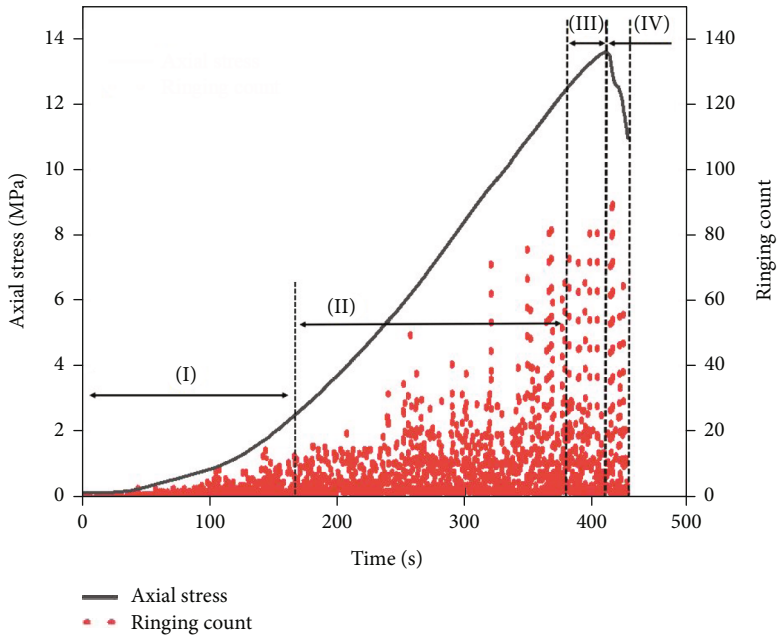

(c) Loading rate 0.03 mm/s

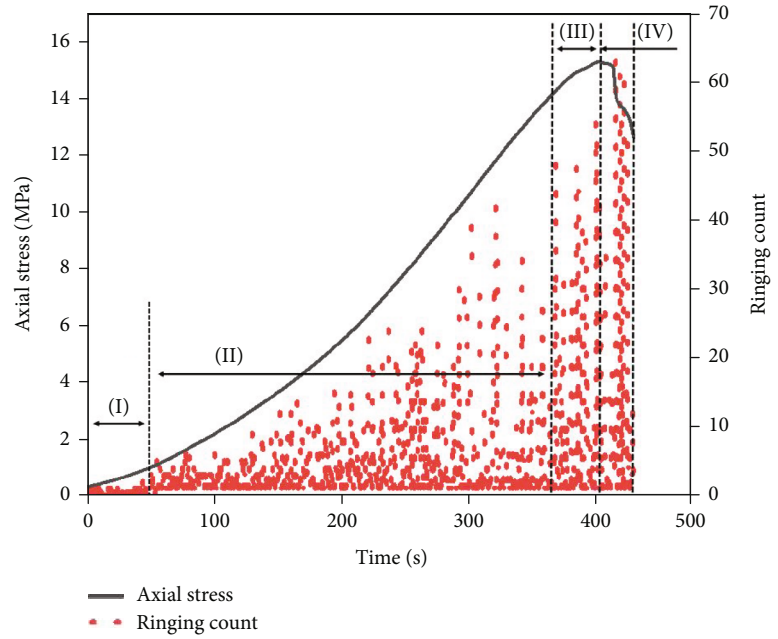

(d) Loading rate 0.05 mm/s

Figure 12: Stress and ring count curves with time during uniaxial compression of specimens with the fissure inclination angle of 30° under different loading rates.

30° shows a trend of increasing-decreasing-increasing, mainly because the cracking is more fully developed under a high loading rate, the number of cracks gradually increases, and the acoustic emission ring count also increases rapidly. Special attention is paid to specimens compressed at 0.01 mm/s where cumulative ring counts reached their maximum: this phenomenon is related to the fissure filler (42.5 ordinary silicate cement) and fissure surface grouting cementing body occlusion mode, which, under pressure, causes the lower end of the fissure surface gradually form a macrocrack, so the energy generated is larger and more concentrated. The overall cumulative ring count of the crack inclination 45° specimen is smaller than that in specimens with a crack inclination of 30° and decreases with the increase of loading rate because these lead to the gradual change of the damage to the specimen grouting surface from compressive to shear damage, the cracks are concentrated in the crack surface, the crack development time inside the specimen is short, the crack expansion is not sufficient to cause failure, the acoustic emission signal is

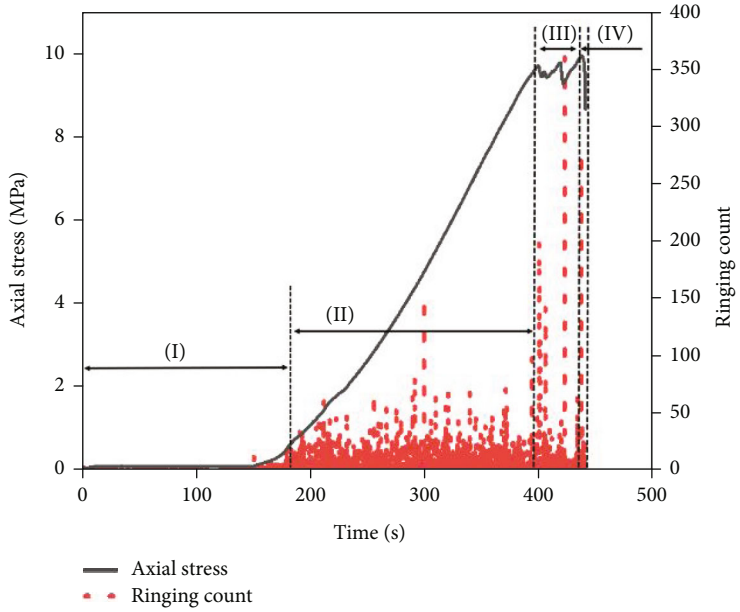

(a) Loading rate 0.005 mm/s

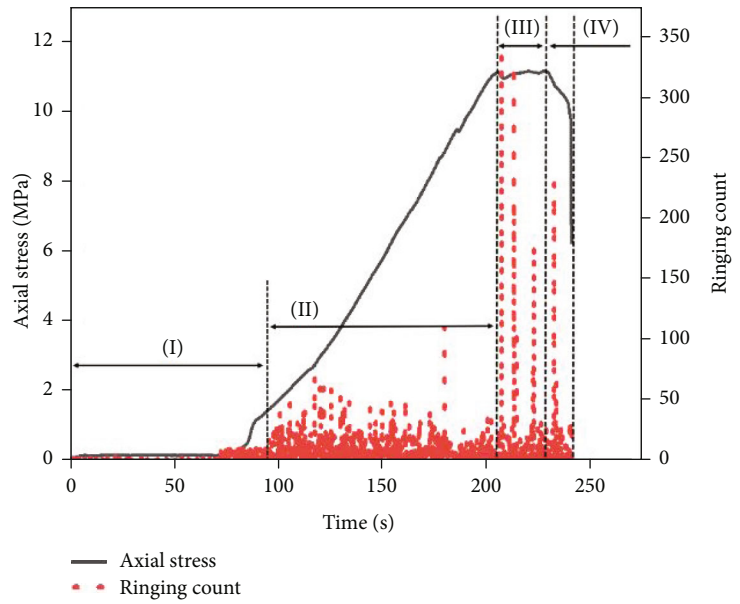

(b) Loading rate 0.01 mm/s

Figure 13: Continued.

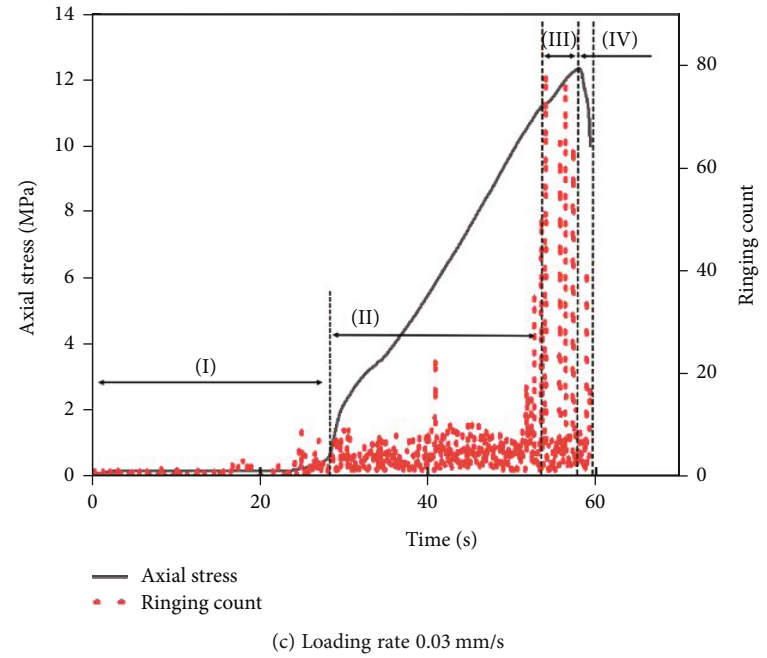

(c) Loading rate 0.03 mm/s

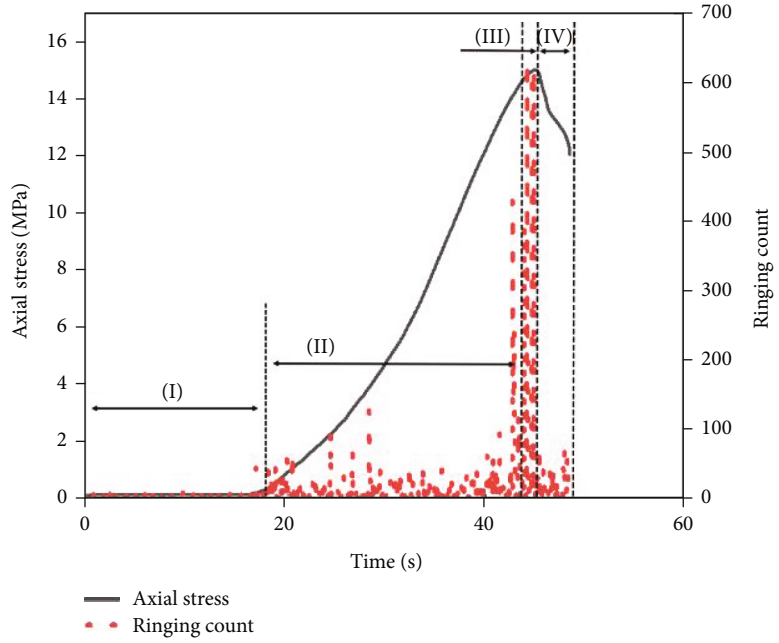

(d) Loading rate 0.05 mm/s

Figure 13: Stress and ring count curves with time during uniaxial compression of specimens with the fissure inclination angle 45° under different loading rates.

inactive, and finally, the specimen undergoes transient damage and rapid slip; accordingly, the cumulative acoustic emission ring count is relatively small.

4. Discussion and Analysis

From the above test results, the crack concentration area of the grouted specimen is found to be closely related to the crack inclination angle, and the loading rate only plays a role in improving the strength of the specimen and promoting the expansion of the crack development. The degree of influence on the damage of the grouted specimen is much smaller than the degree of influence of the crack inclination angle on its strength and damage mode.

Combined with the dynamic mechanical properties of the grouted specimens under uniaxial compression (Figure 15), it can be seen that the grouted body mainly includes the axial crack damage of the intact rock mass (the specimens with the crack inclination angles of 0°, 15°, and 30°), the axial damage to the intact rock mass evolving into the mixed damage of shear breaking along the crack face and the direct shear slip deformation tangentially along

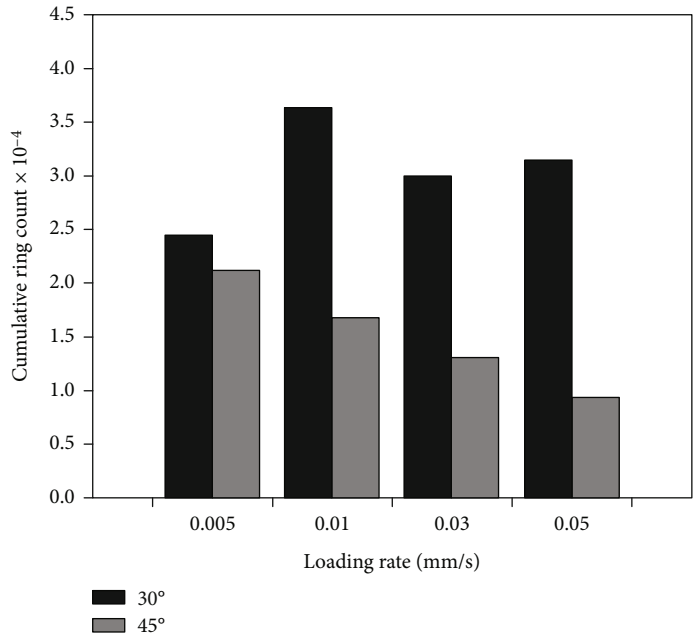

Figure 14: Comparison of cumulative ring counts of specimens with the crack inclination angles of 30° and 45° under different loading conditions.

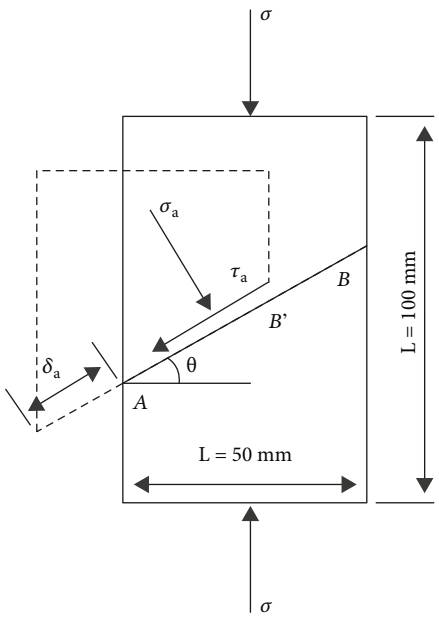

Figure 15: Physical model of grouting with one through-crack inclination.

the crack face (the specimens with the crack inclination angles of 45° and 60°), and the component of compression closure deformation normal to the crack face in the direction of maximum principal stress [41], so this section will mainly discuss the first two forms of damage in cases of different crack inclinations.

The stress-strain curves of specimens with a displacement rate of 0.01 mm/s and crack inclination angles of 0°, 15°, 30°, 45°, and 60° were selected for analysis (Figure 16). The stress-strain curves of the five different fissure inclination slurry bodies have a similar trend, where the peak total strain of the fissure inclination 60° specimen is the smallest, mainly due to the fact that under the uniaxial compressive stress as shown in Figure 16, the fissure inclination 60° slurry surface is mainly subjected to shear action, which is unlikely to produce axial splitting cracks (Figure 8). The deformation of the specimen occurs only at the grouting surface, mainly by the grouting surface bearing the applied pressure, so the crack generation does not involve the upper and lower rock blocks of the grouting surface, while the time to loss of bearing capacity is very short, so the total peak strain is small, for the specimen with the crack inclination angle of 45°, under the action of axial load, although there is no direct shear damage along the grouting surface, but there are axial cracks occurring along the ends of the crack surface, and the later shear cracks occur along the grouting surface, indicating that the crack inclination 45° specimen as a whole is also under load, while the point of load application is gradually transformed to the grouting surface, so that the compressive stress is decomposed, resulting in the peak total strain being greater than that of the specimen with the crack inclination angle of 60°. However, when the crack inclination angle is 0°, 15°, or 30°, under the action of axial load, the cracks mainly penetrate downwards, through the grouting surface to form axial splitting cracks, and no obvious shear cracks are formed inside the grouting surface; therefore, it does not cause significant slip damage along the grouting surface, and the damage pattern is similar to that of the intact specimens, with varying degrees of increase in peak total strain for specimens with the crack inclination angles of 0°, 15°, and 30°.

To study the effects of the crack inclination angle on the peak strength and damage mode of the grouted specimens,

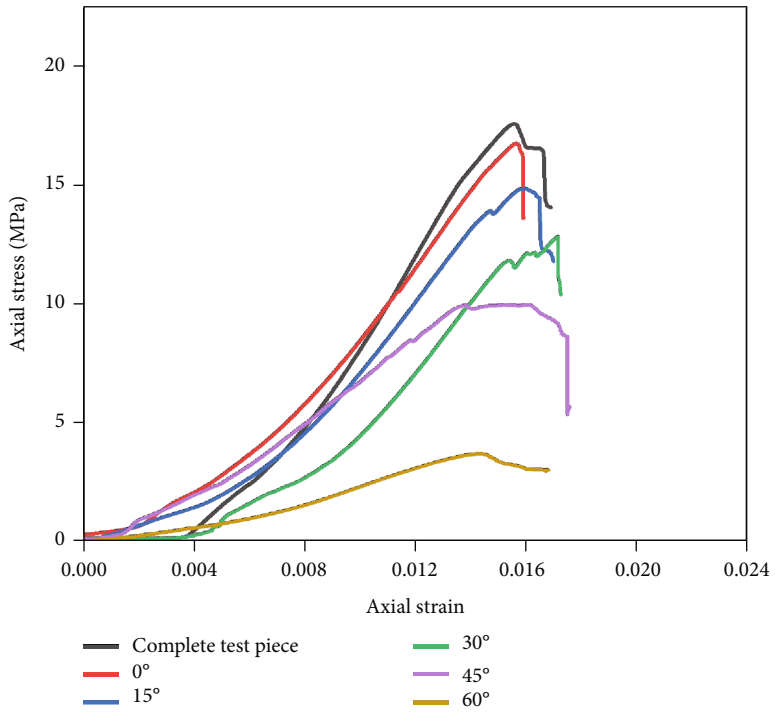

Figure 16: Uniaxial compressive stress-strain curves for specimens with different crack inclination angles.

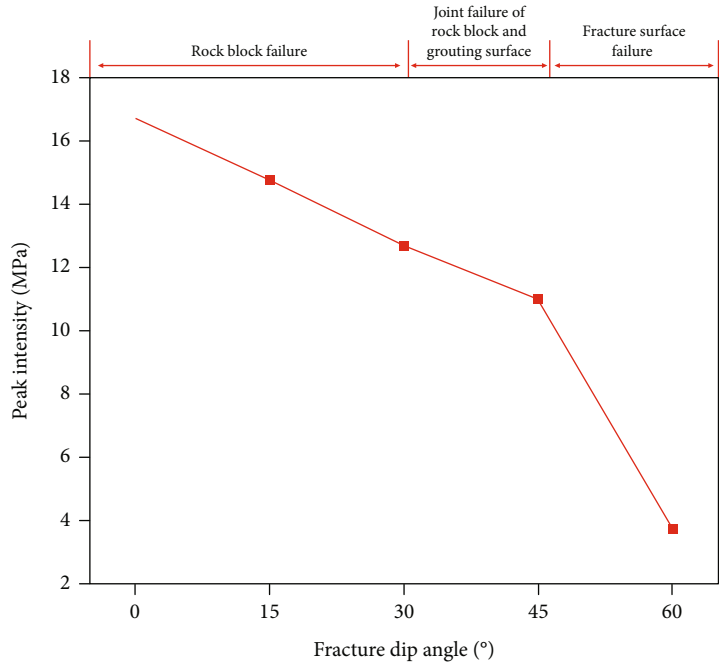

Figure 17: Variations in peak strengths of grouted specimens with the crack inclination angle.

the variation of the peak strength of the specimens with the crack inclination angle is shown in Figure 17. With the change of the crack inclination angle, the specimen strength and damage mode will be divided into three stages, i.e., a rock block damage stage, rock block and grouting surface joint damage stage, and crack surface damage stage. When the crack inclination angle is 0°, 15°, or 30°, the peak strength of the specimen is close to the intact rock, and the mode of damage involves the formation of axial cracks in the intact rock mass. When the crack inclination angle is 45°, with the crack inclination angle increases the strength gradually decreases, the mode of damage involves the axial splitting damage of the intact rock block evolved into a mixed mode of damage along the crack surface which cracks under shear;

when the crack inclination angle is 60°, the strength of the specimen shows a significant decrease and reaches a minimum (of about 3.7 MPa), the failure mode involves shear splitting along the grouting crack surface, and the intact rock block at the upper and lower end of the crack surface has no obvious cracks.

5. Conclusions

(1) Using self-designed molds for grouting reinforcement of rock containing fully penetrated fissures, the overall grouting results are better. The crack inclination angle and loading rate have a significant effect on the mechanics of the crack grouted body and the location of crack formation. Under the same loading conditions, the peak strength of the grouted body shows a decreasing trend with the increase in the inclination angle of the added fissure. The crack inclination angle is 0°, 15°, or 30° in specimens wherein the mode of damage is mainly formed in the upper and lower rock block axial cracks and is closer to that in intact rock specimens upon suffering damage. The damage mode of the specimen with the crack inclination of 45° involves the axial splitting of the intact rock mass evolving into the mixed damage of shear breaking along the crack surface. The damage mode of the specimen with a crack inclination angle of 60° is mainly concentrated on the grouting surface and produces shear slip damage along the grouting crack surface. A critical value of 45° for the crack inclination causes the grout body to break through cracking under load and concentrates the stress inside the grouted solid body

(2) Combined with conclusion (1), the specimens with crack inclination angles of 30° and 45° are used as examples for the fine view damage analysis of the fissure grouted body specimens under the same loading rate conditions. The results show that the initial crack of the crack inclination 30° specimen causes damage with the increase of load in the shape of Chinese capital letter "八" (meaning eight) from the upper end of the crack surface to the lower end of the crack surface as it expands. The initial cracks of the specimens with 45° crack inclination are mainly produced around the crack surface and gradually expand to the inner part of the grout surface with the increase of loading time, and the cracks are terminated at the grout surface

(3) As the loading rate increases, the acoustic emission ring count data of the specimen with a crack inclination of 30° mainly shows a growing trend throughout, mainly because the crack development is more complete, the strain energy is continuously released during the elastic deformation process, and the cumulative ring count gradually rises. At a crack inclination angle of 45°, specimens in the elastic stage (II) have a ring count with almost zero growth, but in the yielding stage (III) and postpeak stage (IV), ring count growth is larger, and the cumulative ring count increases. This acoustic emission response characteristic phenomenon has been theoretically explained and can provide early warning precursors in dynamic hazards after the construction process of joint crack grouting reinforcement

(4) At a given load rate, the peak total strain values of the specimens with the crack inclination angles of 0°, 15°, and 30° are greater than those of specimens with the crack inclination angles of 45° and 60°. The above experimental results are better illustrated by the effects of the crack inclination angle on the peak strength and damage mode of the grouted specimen, which divides the damage mode of the specimen into three stages: a rock block damage stage, rock block and grouting surface joint damage stage, and a crack surface damage stage

Data Availability

Data are available upon request.

Conflicts of Interest

The authors declare that they have no conflicts of interest.

Acknowledgments

This work was financially supported by the Natural Science Foundation of Hebei Province (Grant Nos. E2020402075 and E2022402014), funded by the Science and Technology Project of Hebei Education Department (Grant No. QN2022027), supported by the open fund (PLN2022-21) of State Key Laboratory of Oil and Gas Reservoir Geology and Exploitation (Southwest Petroleum University), and supported by the Guangdong Provincial Key Laboratory of New and Renewable Energy Research and Development (Grant No. E239kf0601).

References

[1] S. C. Bandis, A. C. Lumsden, and N. R. Barton, "Fundamentals of rock joint deformation," *International Journal of Rock Mechanics and Mining Sciences & Geomechanics Abstracts*, vol. 20, no. 6, pp. 249–268, 1983.

[2] Y. Wang, Z. Y. Song, T. Q. Mao, and C. Zhu, "Macro-meso fracture and instability behaviors of hollow-cylinder granite containing fissures subjected to freeze–thaw–fatigue load," *Rock Mechanics and Rock Engineering*, vol. 55, no. 7, pp. 4051–4071, 2022.

[3] H. Cambefort, "The principles and applications of grouting," *GeoScienceWorld*, vol. 10, no. 2, pp. 57–95, 1977.

[4] N. Turk and W. R. Dearman, "Assessment of grouting efficiency in a rock mass in terms of seismic velocities," *Bulletin of the International Association of Engineering Geology*, vol. 36, no. 1, pp. 101–108, 1987.

[5] A. Zolfaghari, A. Sohrabi Bidar, M. R. Maleki Javan, M. Haftani, and A. Mehinrad, "Evaluation of rock mass improvement due to cement grouting by Q-system at

Bakhtiary dam site," *International Journal of Rock Mechanics and Mining Sciences*, vol. 74, pp. 38–44, 2015.

[6] F. Jorne and F. M. A. Henriques, "Evaluation of the grout injectability and types of resistance to grout flow," *Construction and Building Materials*, vol. 122, pp. 171–183, 2016.

[7] S. J. Wei and P. F. Gou, "Analogy simulation test on strengthening effect for pretention of bolts on anchorage body," *Journal of China Coal Society*, vol. 37, no. 12, pp. 1987–1993, 2012.

[8] S. C. Li, Z. F. Li, F. Sha, R. T. Liu, and S. J. Zhang, "The development of new composite material for the grouting treatment of Ordovician limestone aquifer and performance tests," *Materials Research Innovations*, vol. 19, supplement 1, pp. S1-252–S1-255, 2015.

[9] J. Mirza, M. S. Mirza, V. Roy, and K. Saleh, "Basic rheological and mechanical properties of high-volume fly ash grouts," *Construction & Building Materials*, vol. 16, no. 6, pp. 353–363, 2002.

[10] M. N. Ibragimov, "Soil stabilization with cement grouts," *Soil Mechanics & Foundation Engineering*, vol. 42, no. 2, pp. 67–72, 2005.

[11] M. Eriksson and H. Stille, "A method for measuring and evaluating the penetrability of grouts," in *International Conference on Grouting & Ground Treatment*, New Orleans, Louisiana, United States, 2003.

[12] H. Güllü, A. Cevik, K. M. A. al-Ezzi, and M. E. Gülsan, "On the rheology of using geopolymer for grouting: a comparative study with cement-based grout included fly ash and cold bonded fly ash," *Construction and Building Materials*, vol. 196, pp. 594–610, 2019.

[13] Y. Lu, L. Wang, Z. Li, and H. Sun, "Experimental study on the shear behavior of regular sandstone joints filled with cement grout," *Rock Mechanics and Rock Engineering*, vol. 50, no. 5, pp. 1–16, 2016.

[14] Y. Q. Zhou, Q. Sheng, N. N. Li, and X. Fu, "The relationship between dynamic strength and strain rate and damage to rock materials subjected to dynamic cyclic loading," *Geomechanics and Geophysics for Geo-Energy and Geo-Resources*, vol. 7, no. 3, pp. 1–18, 2021.

[15] H. Le, S. Sun, P. H. Kulatilake, and J. Wei, "Effect of grout on mechanical properties and cracking behavior of rock-like specimens containing a single flaw under uniaxial compression," *International Journal of Geomechanics*, vol. 18, no. 10, 2018.

[16] H. Le, S. Sun, P. H. Kulatilake, and J. Wei, "Effect of grout infilling, flaw thickness and inclination angle on strength and failure pattern of rock-like specimens with single flaw," *Arabian Journal of Geosciences*, vol. 12, no. 22, 2019.

[17] C. Xu, Y. Deng, Z. Li, S. Wang, and C. A. Tang, "Crack propagation from a filled flaw in rocks considering the infill influences," *Journal of Applied Geophysics*, vol. 152, pp. 137–149, 2018.

[18] M. Sharafisafa, Z. Aliabadian, F. Tahmasebinia, and L. Shen, "A comparative study on the crack development in rock-like specimens containing unfilled and filled flaws," *Engineering Fracture Mechanics*, vol. 241, article 107405, 2021.

[19] P. Wu, C. Liang, C. Yanlong et al., "Experimental study on mechanical properties and microcrack fracture of coal specimens under the coupling of loading rate and compression–shear loads," *International Journal of Geomechanics*, vol. 22, no. 4, 2022.

[20] T. Bao, K. Hashiba, and K. Fukui, "Effects of water saturation and loading rate on direct shear tests of andesite," *Journal of Rock Mechanics and Geotechnical Engineering*, vol. 14, no. 2, pp. 653–662, 2022.

[21] W. Weng Lei, Z. S. Zhijun, L. Quansheng, and C. Zhaofei, "Real-time characterization of the grouting diffusion process in fractured sandstone based on the low-field nuclear magnetic resonance technique," *International Journal of Rock Mechanics and Mining Sciences*, vol. 152, article 105060, 2022.

[22] P. F. Shen, G. Li, X. S. Li, B. Li, and J. M. Zhang, "Application of fracturing technology to increase gas production in low-permeability hydrate reservoir: a numerical study," *Chinese Journal of Chemical Engineering*, vol. 34, pp. 267–277, 2021.

[23] P. F. Shen, G. Li, B. Li, and X. S. Li, "Coupling effect of porosity and hydrate saturation on the permeability of methane hydrate-bearing sediments," *Fuel*, vol. 269, article 117425, 2020.

[24] Y. Xing, B. Huang, E. Ning, L. Zhao, and F. Jin, "Quasi-static loading rate effects on fracture process zone development of mixed-mode (I-II) fractures in rock-like materials," *Engineering Fracture Mechanics*, vol. 240, no. 107365, 2020.

[25] S. Kumar, G. Tiwari, V. Parameswaran, and A. das, "Rate-dependent mechanical behavior of jointed rock with an impersistent joint under different infill conditions," *Engineering*, 2022.

[26] Y. Wang, T. Mao, Y. Xia, X. Li, and X. Yi, "Macro-meso fatigue failure of bimrocks with various block content subjected to multistage fatigue triaxial loads," *International Journal of Fatigue*, vol. 163, article 107014, 2022.

[27] Y. Wang, Y. Su, Y. Xia, H. Wang, and X. Yi, "On the effect of confining pressure on fatigue failure of block-in-matrix soils exposed to multistage cyclic triaxial loads," *Fatigue & Fracture of Engineering Materials & Structures*, vol. 45, no. 10, pp. 3356–3372, 2022.

[28] A. Cao, G. Jing, Y.-l. Ding, and S. Liu, "Mining-induced static and dynamic loading rate effect on rock damage and acoustic emission characteristic under uniaxial compression," *Safety Science*, vol. 116, pp. 86–96, 2019.

[29] T. Ai, R. Zhang, and J. F. Liu, "Space-time evolution rules of acoustic emission location of unloaded coal sample at different loading rates," *International Journal of Mining Science and Technology*, vol. 22, no. 6, pp. 847–854, 2012.

[30] Y. Jiang, H. Luan, W. Dong, C. Wang, and W. Han, "Failure mechanism and acoustic emission characteristics of rock specimen with edge crack under uniaxial compression," *Geotechnical and Geological Engineering*, vol. 37, no. 3, pp. 2135–2145, 2019.

[31] J. Wu, M. Feng, G. Han, B. Yao, and X. Ni, "Loading rate and confining pressure effect on dilatancy, acoustic emission, and failure characteristics of fissured rock with two pre-existing flaws," *Comptes Rendus-Mécanique*, vol. 347, no. 1, pp. 62–89, 2019.

[32] H. Xunjian, L. Lina, L. Gang, G. Xiaonan, H. Guo Panpan, and M. J. Haibo, "Cracking behavior and acoustic emission characteristics of rock containing a single preexisting flaw," *Shock and Vibration*, vol. 2021, Article ID 7117163, 15 pages, 2021.

[33] X. Wang, E. Wang, X. Liu, and X. Zhou, "Failure mechanism of fractured rock and associated acoustic behaviors under different loading rates," *Engineering Fracture Mechanics*, vol. 247, no. 16, article 107674, 2021.

[34] A.S.T.M. Standard, *D7012, Standard Test Method for Compressive Strength and Elastic Moduli of Intact Rock Core Specimens under Varying States of Stress and Temperatures*, ASTM International, West Conshohocken, 2014.

[35] X. W. Zhou, *Grouting Construction Manual*, Coal Industry Press, Beijing, 1st edition, 2014.

[36] Q. Yin, H. W. Jing, and H. J. Su, "Strength degradation and loading rate effect of sandstone containing a longitudinal fissure," *Journal of Mining & Safety Engineering*, vol. 33, no. 1, pp. 128–133, 2016.

[37] G. Z. Sun, *Mechanics of Rock Mass Structure*, Science Press, Beijing, 1st edition, 1988.

[38] W. Zhao, Z. Wang, Z. Song, P. G. Ranjith, H. Zhang, and T. Wang, "Experimental exploration of damage propagation in rocks using acoustic emission," *Bulletin of Engineering Geology and the Environment*, vol. 80, no. 8, pp. 6065–6075, 2021.

[39] L. Zongze, F. Yang, F. Jinyang, J. Deyi, and A. Julien, "Fatigue effects of discontinuous cyclic loading on the mechanical characteristics of sandstone," *Bulletin of Engineering Geology and the Environment*, vol. 81, no. 8, 2022.

[40] J. Yang, Z. Kang, S. Yufeng et al., "Acoustic emission characteristics and fractal evolution of rock splitting and failure processes under different loading rates," *Arabian Journal of Geosciences*, vol. 15, no. 3, 2022.

[41] P. H. S. W. Kulatilake, J. Liang, and H. Gao, "Experimental and numerical simulations of jointed rock block strength under uniaxial loading," *Journal of Engineering Mechanics*, vol. 127, no. 12, pp. 1240–1247, 2001.